crystals

MDPI

Article

Highly Visible Photoluminescence from Ta-Doped Structures of ZnO Films Grown by HFCVD

Víctor Herrera [1], Tomás Díaz-Becerril [1,*], Eric Reyes-Cervantes [2], Godofredo García-Salgado [1], Reina Galeazzi [1], Crisóforo Morales [1], Enrique Rosendo [1], Antonio Coyopol [1], Román Romano [1] and Fabiola G. Nieto-Caballero [1]

[1] Centro de Investigación en Dispositivos Semiconductores, Universidad Autónoma de Puebla, 14 sur y Av. San Claudio, C.U., Edif. IC-5, Puebla 72570, Mexico; pds_vherrera@hotmail.com (V.H.); godgarcia@yahoo.com (G.G.-S.); ingquim25@gmail.com (R.G.); crisomr@yahoo.com.mx (C.M.); enrique171204@gmail.com (E.R.); acoyopol@gmail.com (A.C.); roman.romano@gmail.com (R.R.); ruscaballero@yahoo.com.mx (F.G.N.-C.)

[2] Centro Universitario de Vinculación y Transferencia de Tecnología, Prol. de la 24 sur esq. con Av. San Claudio, C.U., Edif. CUVyTT, Puebla 72570, Mexico; eric.cervantes@correo.buap.mx

* Correspondence: tomas.diaz.be@gmail.com; Tel.: +52-222-229-5500 (ext. 7871)

Received: 27 July 2018; Accepted: 3 September 2018; Published: 22 October 2018

Abstract: Tantalum-doped ZnO structures (ZnO:Ta) were synthesized, and some of their characteristics were studied. ZnO material was deposited on silicon substrates by using a hot filament chemical vapor deposition (HFCVD) reactor. The raw materials were a pellet made of a mixture of ZnO and Ta_2O_5 powders, and molecular hydrogen was used as a reactant gas. The percentage of tantalum varied from 0 to 500 mg by varying the percentages of tantalum oxide in the mixture of the pellet source, by holding a fixed amount of 500 mg of ZnO in all experiments. X-ray diffractograms confirmed the presence of zinc oxide in the wurtzite phase, and metallic zinc with a hexagonal structure, and no other phase was detected. Displacements to lower angles of reflection peaks, compared with those from samples without doping, were interpreted as the inclusion of the Ta atoms in the matrix of the ZnO. This fact was confirmed by energy dispersive X-ray spectrometry (EDS), and X-ray diffraction (XRD) measurements. From scanning electron microscopy (SEM) images from undoped samples, mostly micro-sized semi-spherical structures were seen, while doped samples displayed a trend to grow as nanocrystalline rods. The presence of tantalum during the synthesis affected the growth direction. Green photoluminescence was observed by the naked eye when Ta-doped samples were illuminated by ultraviolet radiation and confirmed by photoluminescence (PL) spectra. The PL intensity on the Ta-doped ZnO increased from those undoped samples up to eight times.

Keywords: zinc oxide; tantalum oxide; ZnO:Ta doped films; substitutional alloy

1. Introduction

In recent years, ZnO has become one of the most closely studied materials, due to its very interesting properties in optoelectronic devices applications, such as room temperature lasers [1], light emitting diodes [2,3], ultraviolet (UV) detectors [4], field-emission displays [5,6], photonic crystals [7], solar cells [8–10], and sensing in the nano-size range [11,12]. The control of its properties is critical in the context of novel applications. For this reason, a better understanding of the synthesis of microstructures/nanostructures with different morphologies is important and necessary to achieve objectives and applications on materials for the modern world [13].

Several techniques have been employed to make ZnO in thin films and nano- or microstructures; among them are radio-frequency magnetron sputtering, pulsed laser deposition, spray pyrolysis,

and thermal evaporation flame synthesis [14–17]. The properties of the materials seem to be dependent on the process and technique used to synthesize them. Developing new or modified methods to obtain those type of materials could report new insights on topics that are not yet understand for those types of oxides.

A profitable, simple, and easily scalable method to synthesize the material the hot filament chemical vapor deposition (HFCVD). This technique allows us to produce multifunctional structures on a larger scale. In addition, it is possible to control the material properties by only changing the synthesis conditions.

This technique has been used to grow a wide variety of films, including diamond [18], as well as amorphous silicon nitride [19,20], semiconductor compounds [21], and more. Recently, the technique has been used to grow several nanostructures of different materials, such as silicon-rich oxides [22], nanocrystalline silicon [23], graphene [24], molybdenum selenide [25], silicon carbide [26], and zinc sulfide [27] among others, for applications in new or improved devices, such as solar cells, sensors, and metal oxide semiconductors (MOS) structures [18,23]. HFCVD technology is compatible with the current silicon-based technology, and it has advantages over other methods because it can produce materials at low cost, and on a wide substrate surface.

An important issue regarding applications in electronic and optoelectronic technologies is doping. ZnO exhibit naturally n-type conductivity because the presence of punctual defects, such as zinc interstitial and/or oxygen vacancies in its matrix [28,29]. P-type is not easy to obtain, due to the compensation effect that impedes this [3,29]. However, some other properties, such as optical emission can be changed when ZnO is doped. It is reported light emission, in the UV-visible range, can be obtained when the material is doped with transition metals.

It has been reported that green emission occurs at around 510 nm when copper atoms are incorporated in ZnO films [30–32]. The luminescence was ascribed mainly to the existence of oxygen vacancies. Other transition metals when introduced to ZnO, such as Al, Li, Co, Mn, and Zn, have also been reported to exhibit emissions in different ranges; however, the wavelengths of emission and intensity depended on the process and technique of the growth [10,33–35]. Similarly, yellow emission was been observed when the ZnO synthesis was performed by chemical techniques. This emission was assigned to the existence of oxygen interstitials [36].

Ta is an atom that has been introduced in ZnO to change the properties of the material. It was found that the Ta atoms can substitute Zn atoms in the ZnO matrix, modifying the electrical and optical properties of the films. Some uses include photoactinic and TCO (transparent and conductive oxide) uses, among others. However, information on the changes on the photoluminescent properties with the incorporation of Ta in the ZnO material is missing.

To investigate on the effect of ZnO doping with Ta atoms, core-shell structures doped with tantalum were fabricated by the HFCVD method, and the optical (photoluminescence), structural, morphological, and electrical properties were studied and reported. By comparison, the undoped structures were also prepared, to observe the effect of the dopant.

The results showed that the properties of ZnO core-shell structures are a bit different from those of pure ZnO crystals. Photoluminescence (PL) intensity on Ta-doped ZnO increased from those undoped samples by up to eight times. This effect was ascribed to a change in the morphology of the structures, with the incorporation of tantalum in the process. The morphology of the structures in this work was found to be modified with the incorporation of tantalum in the process; this effect increases the specific area of the material, increasing the number of radiative centers.

Tantalum atoms do not appear to introduce additional radiative centers that contribute to the PL, but they affect the electricals of the ZnO grains. Ta is a donor in ZnO that contributes to reduce the resistivity of the ZnO grains in the shell. The results are in concordance with other authors.

2. Materials and Methods

Films obtained in this work were grown using a hot filament chemical vapor deposition system (HFCVD). The experimental homemade reactor consisted of elements showed in Figure 1. As can be seen in the figure, the system has a 2-way valve to introduce a reactant gas into the chamber, such as hydrogen or nitrogen; in this work, molecular hydrogen was only used as reactant to grow the films. Also, the system has a flowmeter and a pressure valve to control gases into the chamber; in this work, the reaction chamber was saturated with hydrogen, and the temperature in the substrate was kept at 800 °C.

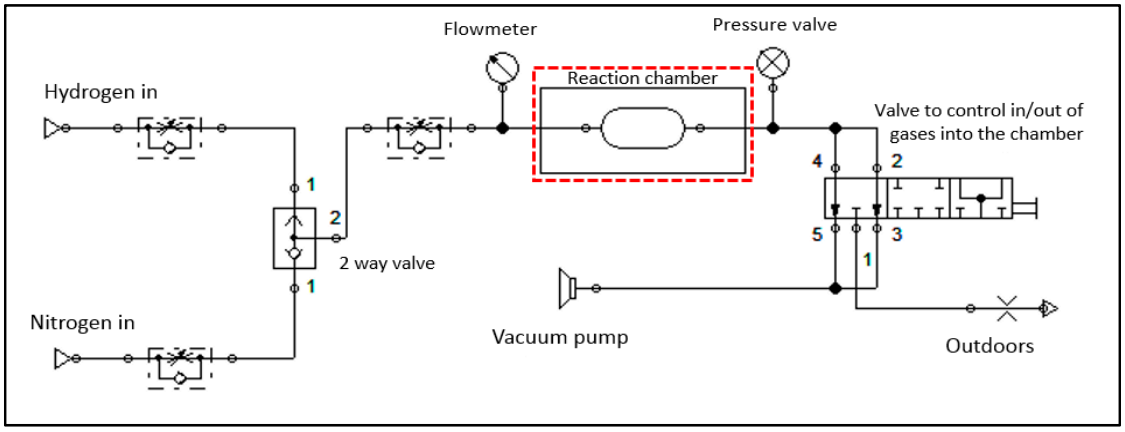

Figure 1. Schematic diagram of the hot filament chemical vapor deposition (HFCVD) homemade system used to grown films in this work.

The reaction chamber (red box in Figure 1) consists of a cylindrical tube of quartz that was selected to support elevated temperatures in its interior. The tube has metal caps of stainless steel and O-rings at each end to ensure complete isolation between the inside of the tube under atmosphere, owing to elevated temperatures, reactant gases are highly pyrophoric. Principal components inside the reaction chamber are shown in Figure 2, and a sprinkler of stainless steel was used to fill the reaction chamber with the reactant gas. A filament of tungsten was used to raise the temperature inside the reaction chamber; in this work, the filament was fixed at 2000 °C. A pellet fabricated with a mixture of powders of ZnO (Mallinckrodt Chemicals CAS 1314-13-2, St. Louis, MO, USA) and Ta_2O_5 (ALDRICH CAS 1314-61-0, St. Louis, MO, USA) was used as a precursor to obtain the ZnO and ZnO:Ta doped films. The amount of ZnO powder was kept in 500 mg, and the amount of tantalum oxide was varied by a percentage of 0%, 10%, 20%, 40%, 50%, and 60%, for 500 mg of ZnO, i.e., 500 mg ZnO + 0 mg Ta_2O_5, 500 mg ZnO + 50 mg Ta_2O_5, 500 mg ZnO + 100 mg Ta_2O_5, and so on. After having the required weights of each powder, both powders of ZnO and Ta_2O_5 were mixed until a homogenous powder was obtained. After that, each mix was 1 ton-pressed. A disk shape of 10 mm in diameter and 5 mm in height were the result. All films were grown on a silicon n-type substrate.

The grown process was as follows: the reactor was sealed, and a flow of hydrogen was passed twice through it; next, the hydrogen flow was maintained inside the chamber and the filament is turned on; this process was kept by 3 min.

At a filament temperature of 2000 °C, the molecular hydrogen gas was dissociated into radicals that were highly reactive, which impinged on the pellet that was used as the source to produce intermediaries, such as Zn (vapor), Ta (vapor), and OH principally, although the additional reactions could occur with the gas and the substrate [37]. Finally, by the reactor dynamics, the gases are transported to the substrate where the film is obtained, optical, and structural properties of this were studied by X-ray, SEM, energy dispersive X-ray spectrometry (EDS); the Hall Effect, and PL techniques.

The crystalline structure and the orientation of the crystallites were studied using X-ray diffraction (BRUKER D8 with Cu Kα radiation (λ = 1.541 Å), Billerica, MA, USA); Raman spectra were taken

with a RAM HR800 Raman spectrometer (HORIBA, Les Ulis, France) equipped with an Olympus BX41 microscope (Olympus, Tokyo, Japan); a 632.8 nm He-Ne laser was used as the excitation source. The surface morphology and composition of the films were examined with two systems; the low resolution was taken with a system SEM Jeol model 6610LV (JEOL Ltd., Tokyo, Japan) equipped with an INCA energy dispersive X-ray attached to this, and the high resolution was analyzed with a field emission scanning electron microscope, FESEM JSM 5400LV (JEOL Ltd., Tokyo, Japan) equipped with a NORAN energy dispersive X-ray spectrometer. The profilometry and roughness analyses of the films were taken with a surface profiler Dektak 150 (Veeco Instruments, Inc., Plainview, NY, USA). Photoluminescence measurements were performed at room temperature with a spectrofluorometer FluroMax 3 (Horiba, Ltd., Kyoto, Japan) that was equipped with an emission detector with high sensibility and a 150 W xenon lamp to excite the samples. The electrical properties of the films were determined with a Hall Effect system from Ecopia Company, model HMS-5000 (Ecopia, Waterloo, ON, Canada), using a magnetic field of 0.5 T.

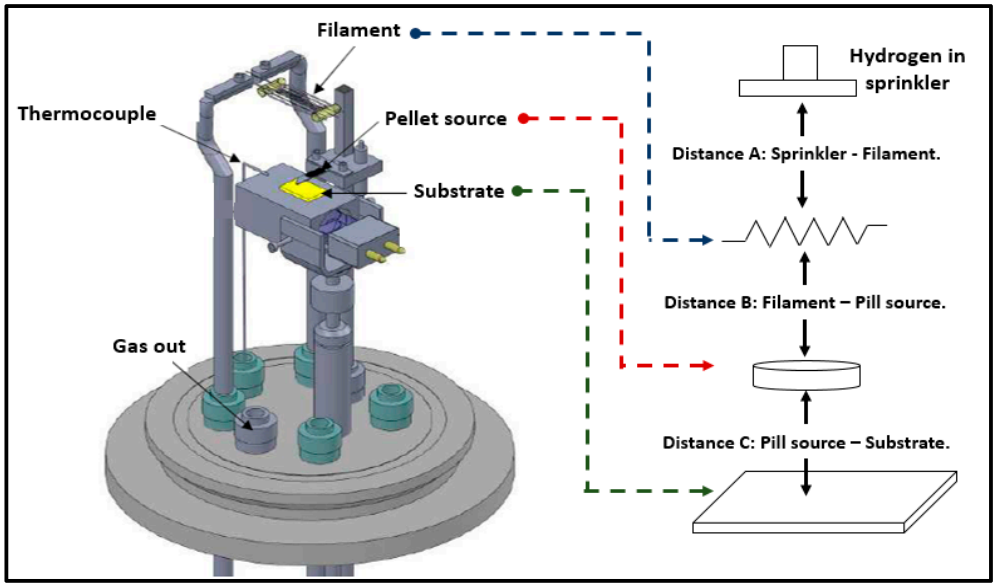

Figure 2. The principal components inside of the reaction chamber.

3. Results and Discussion

3.1. Structural Characterization by XRD

The diffractograms of the films of polycrystalline zinc oxide doped with tantalum are shown in Figure 3, and a pure spectrum of ZnO is presented as a reference. For the pure ZnO material (Figure 3a), the presence of the diffraction peaks indicated that the material possessed a polycrystalline structure. Three well-distinguished diffraction peaks placed at 2θ = 32°, 34.6°, and 36.4°, corresponding to planes (100), (002), and (101) were identified and matched with a hexagonal (wurtzite) ZnO crystalline structure (pdf card 075-0576). Additionally, some other diffractions peaks could be seen at 2θ = 47.8°, 56.8°, 63.1°, 68.0°, and 69.3°, corresponding to reflections on (102), (110), (103), (112), and (201) planes of wurtzite ZnO structure respectively. The presence of the Zn phase was identified by the peaks placed at 2θ = 39.2°, 43.3°, and 54.5°, corresponding to planes (100), (101), and (102) of Zn in the hexagonal phase (pdf card 004-0831).

The diffraction peaks from the ZnO:Ta samples are presented in Figure 3b–f. Some differences can be seen from that of reference sample (Figure 3a). As can be observed, the peak of ZnO in 2θ = 69.3° was could not peak in the other range; to get a better view of other peaks, we plotted the same diffraction patterns in a range from 2θ = 30° to 66° in Figure 4. In this graphs, it was possible to observe an additional diffraction peak arising at 2θ = 66.98° corresponding to the structure of

$ZnTa_2O_6$, suggesting some that Ta atoms were incorporated into the ZnO lattice (pdf card 049-0746) [38]. Because the atomic radii of Ta (0.78 Å) are very similar to Zn atoms (0.82 Å) these atoms easily replace some zinc atoms in the ZnO network without making abrupt changes in the ZnO lattice. In us case, a small level expansive stress in the ZnO lattice can be observed in 2θ = 63.1, corresponding to the plane (103); this stress caused this peak to shift to lower angles (red arrows in Figure 4c,d), but this peak could not be observed clearly in all diffractions [39,40].

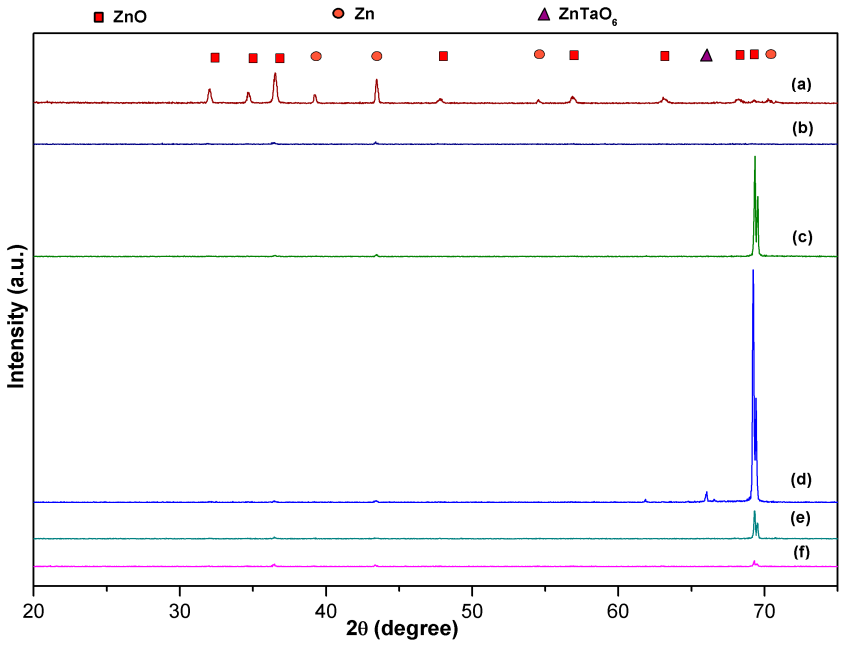

Figure 3. X-ray diffraction (XRD) patterns for (**a**) undoped ZnO film, and ZnO:Ta-doped films grown with a pellet weight of (**b**) 50 mg, (**c**) 100 mg, (**d**) 200 mg, (**e**) 250 mg, and (**f**) 300 mg of Ta_2O_5.

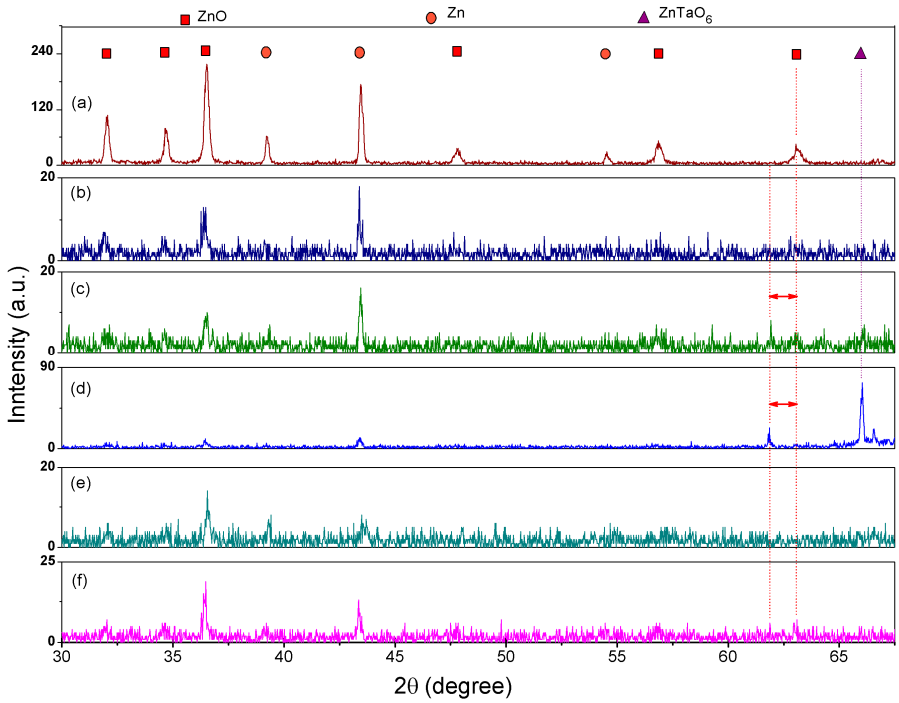

Figure 4. Patterns for (**a**) undoped ZnO film, and ZnO:Ta-doped films grown with a pellet weight of (**b**) 50 mg, (**c**) 100 mg, (**d**) 200 mg, (**e**) 250 mg, and (**f**) 300 mg of Ta_2O_5, in a range of 2θ = 30° to 66°.

It is interesting to note that for the principal peak of ZnO at 2θ = 36.4° in Ta-doped samples corresponding to (101), the plane changed strongly in intensity as the concentration of Ta was increased in the process (Figure 4). This result suggests that the high content of Ta may lead to the degradation of ZnO crystallinity. The other ZnO peaks also became small and broad, which could be an indication that tantalum atoms in the HFCVD process could modify the crystalline orientation of the growth, and from here modify the film morphology.

Diffraction peaks were analyzed with software HighScore Plus of PANalytical, every profile was approximated using a standard Caglioti function with a Pseudo-Voight profile fitting; the results are shown in Table 1.

Table 1. Lattice parameters and crystallite size for ZnO and ZnO:Ta-doped films obtained.

Reference Name	d (Å)	(hkl)	a (Å)	c (Å)	Average Crystallite Size (nm)
ZnO	2.5869	(002)	3.2406	5.1738	224
ZnO 50 mg Ta	2.4653	(101)	3.2361	5.1841	155
ZnO 100 mg Ta	1.3542	(201)	3.2401	5.1806	142
ZnO 200 mg Ta	1.3561	(201)	3.2448	5.1831	134
ZnO 250 mg Ta	1.3546	(201)	3.2407	5.1874	129
ZnO 300 mg Ta	1.3551	(201)	3.2419	5.1895	122

Analyzing the diffraction chart, it can be see the three important diffraction peaks of (100), (002), and (101), the planes of ZnO were diminished, with the introduction of Ta in the ZnO process, which it could mean the growth in that direction is inhibited while the growth along (201) is favored. According to the data obtained and presented in Table 1, it can be seen that the crystallite size of ZnO is bigger than the crystallites of ZnO:Ta doped, because when ZnO is doped with tantalum atoms, the crystallite size decrease strongly, and after this, the crystallite size decreases slowly, in this case, this fact could be an indication that the tantalum atoms are creating this effect.

According to the other reviewed reports, when ZnO is doped with tantalum, the crystallite size is modified, but there is no consensus of the increment or decrement in the crystallite size in ZnO:Ta-doped films; this fact seems to be more greatly affected by the technique used to grow the film; even when ZnO is doped with other materials, the crystallite size sometimes increases, while at other times it decreases [38,40,41]. For example, Bang et al. reported the effect of lithium doping in ZnO films, they found that the (002) planes of ZnO were reduced as the Li content was increased; this was interpreted as a degradation of the ZnO crystallinity, while an increase in the grain size was observed as the concentration of lithium increased [42]. Also, it has been reported that the presence of metallic zinc is associated with the existence of the core-shell structures, where the metallic zinc is the core and the ZnO nanocrystals are comprise the shell [37].

3.2. Raman Measurements

The room temperature Raman spectra for undoped and Ta-doped ZnO in the range of 100 to 1000 cm^{-1} are presented in Figure 5. Three main bands were observed for pure ZnO (Figure 5a). A peak labeled E_2 (High) at 437 cm^{-1} is known as the active optical phonon mode. The vibrational modes at 97 cm^{-1}, known as E_2 (LO) and 570 cm^{-1}, known as A_1 (LO), are also observable on the spectra. The presence of the three observed vibrations, in our measurements, confirmed that the material synthesized had wurtzite hexagonal structure [43–46].

It was reported that a broad Raman band at about 570 cm^{-1} may originate from defects related to the phonon mode, O-vacancy-related stable complexes [47], zinc interstitials, or from the disorder-activated B1 (High) silent mode [48] of w-ZnO.

It is well known that when metallic zinc particles are exposed to air or/and to an oxygen environment, a $Zn_{1+X}O$-defective zinc oxide with a Zn ion in the interstitial position is formed at around the metallic zinc [49], and a broad Raman band with a peak centered at 560 cm^{-1} was seen on the spectra. If it was assumed that the Raman band centered at 563 cm^{-1}, as seen in Figure 5a, had a

contribution due to the formation of a defective oxide, then this result suggests us that our material was a core-shell type, where the core was metallic zinc and the shell consisted of ZnO grains.

Moreover, the undoped and Ta-doped ZnO samples were grown under an oxygen-deficient environment, and therefore, the synthesized material contained a great number of oxygen vacancies and zinc interstitials [29,50,51], and they could also contribute to the broadening of the Raman band observed at 563 cm^{-1}.

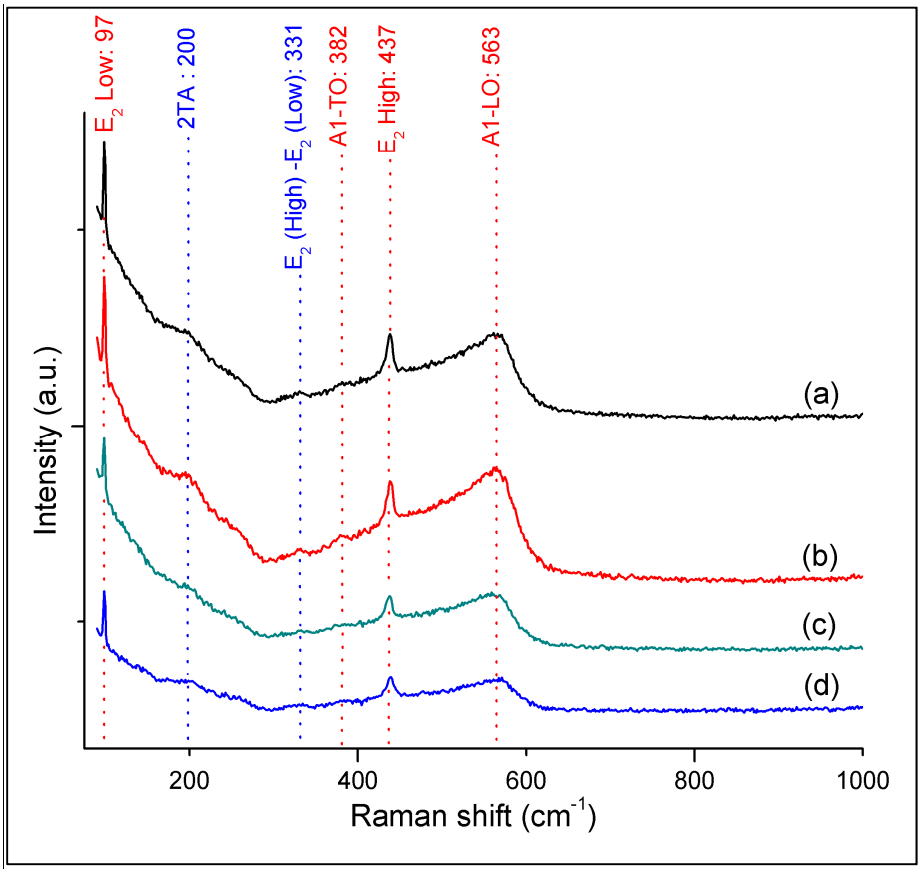

Figure 5. Raman shift from the samples of (**a**) undoped ZnO, and ZnO:Ta-doped films, grown with pellet weight of (**b**) 50 mg, (**c**) 200 mg, and (**d**) 300 mg of Ta_2O_5.

Raman spectra from the Ta-doped ZnO are shown in Figure 5b–d. It can be seen that all of the peaks were found to correspond to that from the undoped sample (Figure 5a); the only difference was the reduction in the intensity of the E_2 (high) vibration, and the broadening of both the second order and A_1 (LO) modes.

This observation could be an indication that Ta is encrusted in the ZnO matrix, and that it induces small disorder in the lattice. The reduced intensity in the E_2 (high) peak might be related to the degradation on the crystalline quality as observed by X-ray diffraction; we can expect those tantalum atoms, when incorporated in the film, to induce change in the bonds strength between zinc and oxygen; therefore crystallinity is affected by this process, as have been observed in XRD results.

3.3. SEM and EDS Studies

Analysis by SEM was carried out to observe the film morphology, and the images are presented in Figure 6. It can be seen the surface morphology changed as the percentage of Ta_2O_5 increased in the pellet source. The picture for undoped ZnO film (Figure 6a) shows a morphology with a high density of big spherical shapes, and both the density and size of these structures reduced or even disappeared

as the Ta_2O_5 content increased in the process (Figure 6b–f). Magnification of these samples (Figure 7) showed the shape details of their morphology.

Micrographs taken on the Ta-doped ZnO samples (Figure 6b–f) showed that the roughness of the surface decreased as the content of Ta_2O_5 was increased in the pellet source; measurements of profilometry were taken over the surface of each film, and the results obtained showed an irregular surface, as can be seen in that Figure 6; the results obtained showed depths with a minimum of 10 µm and a maximum of up to 150 µm, but surface roughness (RMS) analysis performed with this technique showed that surface tended to form a softer surface when the amount of tantalum was greater in the growth process; this RMS factor was plotted and it can be observed in Figure 8.

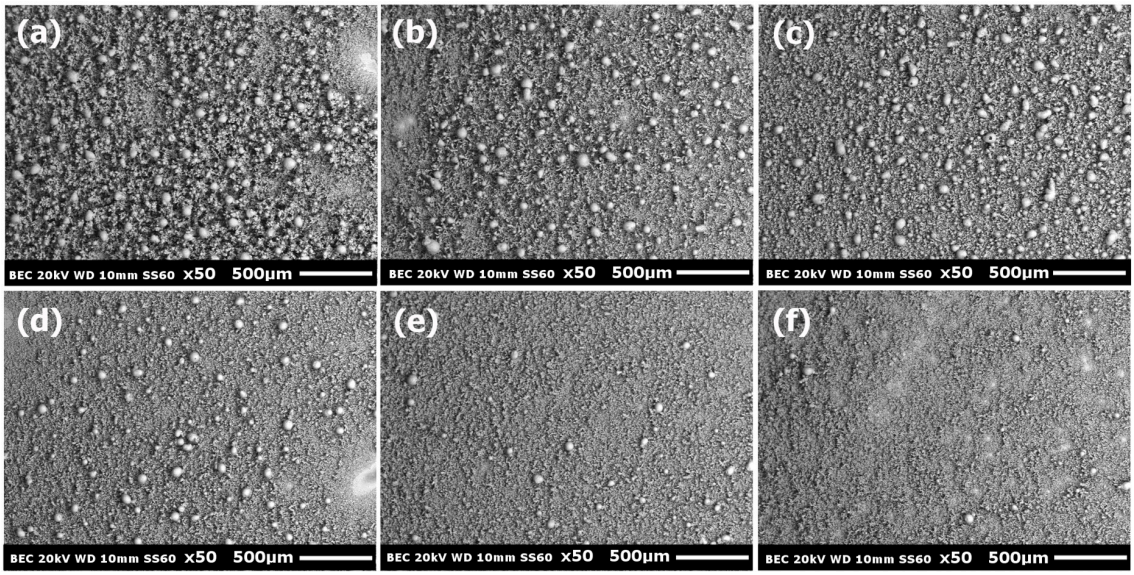

Figure 6. Results of scanning electron microscopy (SEM) 50× of (**a**) undoped ZnO film, and ZnO:Ta-doped films grown with a pellet weight of (**b**) 50 mg, (**c**) 100 mg, (**d**) 200 mg, (**e**) 250 mg, and (**f**) 300 mg of Ta_2O_5.

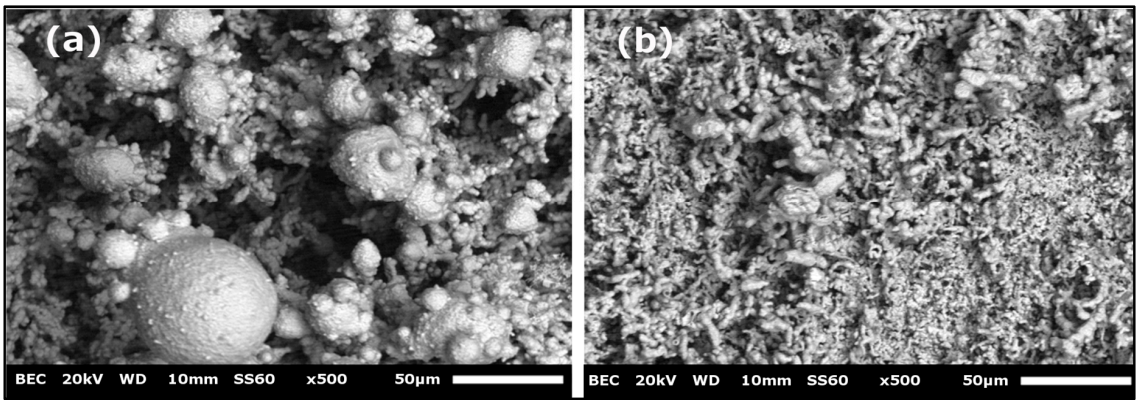

Figure 7. Zoom of 500× on the film of (**a**) ZnO, and (**b**) ZnO:Ta doped with 300 mg of Ta_2O_5 on pellet.

A detailed SEM image from those samples with a 500× zoom is shown in Figure 7. The surface was composed by spheres and rods in a random form like a porous sponge. Additionally, a FESEM analysis of Figure 7a and b displayed the same type of spherical structures, but of different size. Some of those structures seemed hollow or even broken, showing a shell type structure, this shapes could be observed with a high resolution for ZnO in Figure 9(a.1–a.3), and for ZnO:Ta doped in Figure 9(b.1–b.3).

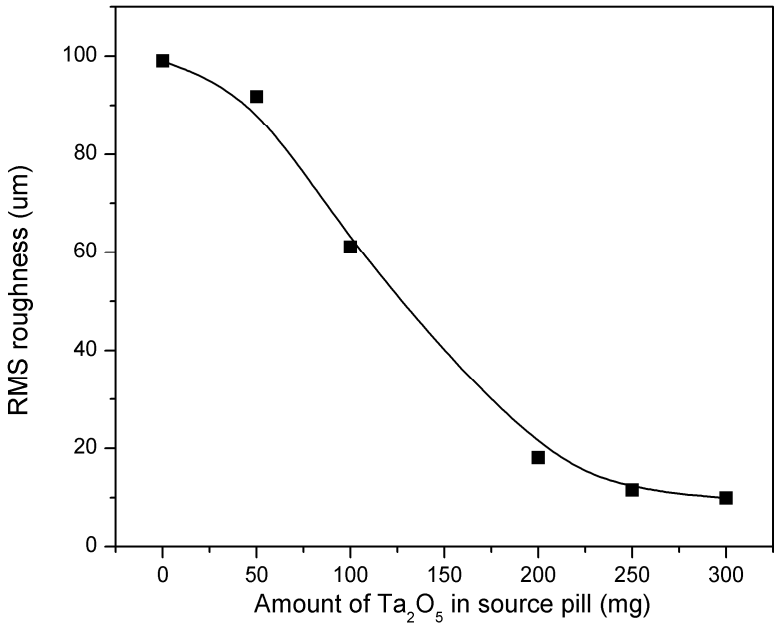

Figure 8. Roughness dependence in films obtained according to the amount of Ta in the source pellet.

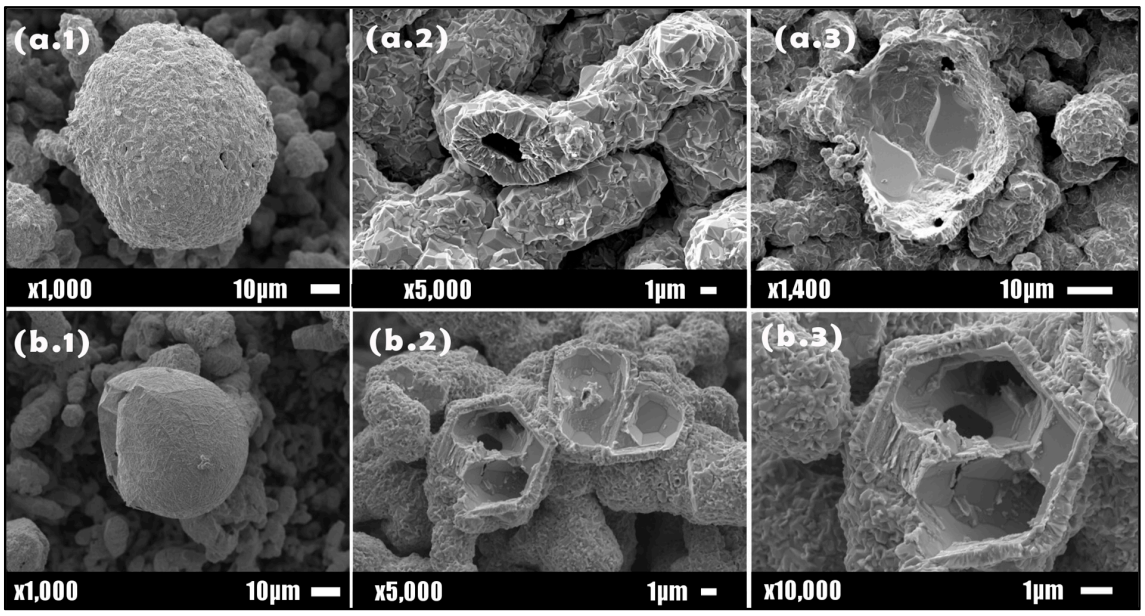

Figure 9. High-resolution field emission (FE) SEM measurements for (**a.1**–**a.3**) undoped ZnO film, and (**b.1**–**b.3**) ZnO:Ta-doped film in different zones of scanning, grown with 300 mg of Ta_2O_5 in the pellet.

From EDS analysis carried out on undoped ZnO films, only oxygen, and zinc elements were detected (Figure 10a). The relation of Zn/O of greater than one indicated that the material was out of stoichiometry, which meant a zinc-rich ZnO material. Our results were in agreement with those found by other authors for this type of systems [37,52,53].

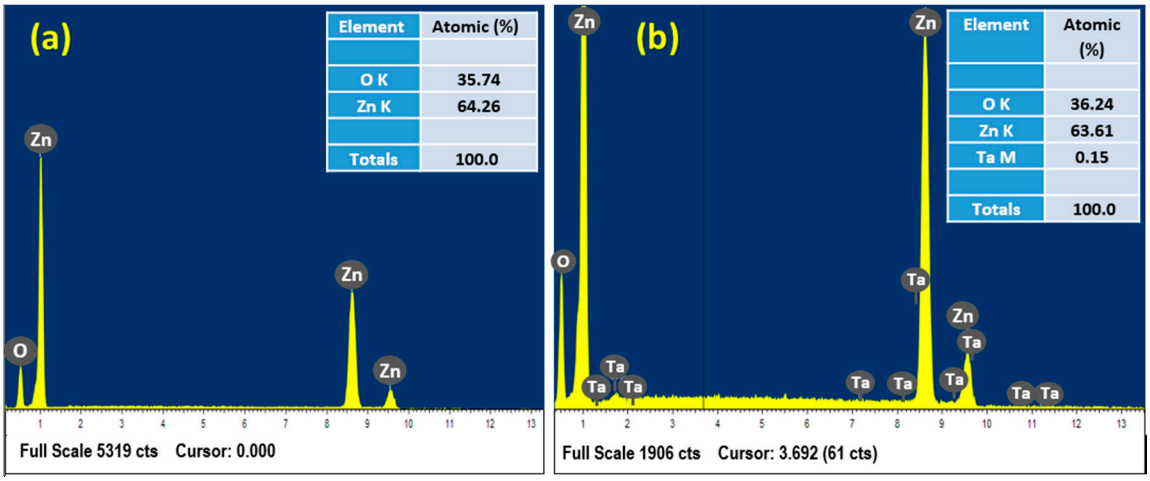

Figure 10. X-ray spectrometry (EDS) analysis for (**a**) undoped ZnO film, and (**b**) ZnO:Ta-doped film grown with 300 mg of Ta_2O_5 in the pellet source.

EDS results on Ta-doped ZnO samples (Figure 10b) indicate that it was a Zn-rich ZnO material, but there was also a clear contribution of the tantalum element around of 0.1% and 0.15% in atomic percentage (±0.5% in weight), this could be owing to the fact that tantalum atoms are mainly incorporated inside the lattice of ZnO, but no over surface of the structures obtained.

The data above could shed some light about the growth process. For undoped ZnO samples, the spheres could be formed as follows. The atomic hydrogen impacted on the pellet source producing OH^- (gas) and Zn (gas) according to the reaction proposed in [37,39]. After that, Zn atoms condensed in a vapor phase, and some Zn liquid drops were formed and they acted as nucleation sites, and OH ions are attached to the surface, forming a mixture of zinc in the liquid state, covered with a thin film of ZnO (solid), and they were deposited on the substrate, where it eventually coalesced and this drop increased in size. Further, due to the presence of OH, the zinc oxide cover increases in thickness, and a core(liquid)–shell(solid) structure was formed because of differences in the melting points 420 °C and 1975 °C for zinc and ZnO respectively.

As the growth was performed at a high temperature, the nuclei remained in a liquid state, producing a Zn gas pressure, due to the vapor–liquid equilibrium, and the Zn atoms diffused through the grain boundaries of the shell to release the internal pressure. Eventually the shell broke and Zn gas escaped, producing holes on the shell, as seen in Figure 9. This effect has been reported in the literature, and concentric core-shell (Zn/ZnO) balls have been synthesized by oxidizing ZnO powders at low temperatures in air, followed by annealing at temperatures above the zinc melting point [39,54,55].

The existence of this crystalline zinc forming the core were detected by X-ray diffraction results (Figure 3) and by EDS, where it obtained a relation Zn/O of 69% at 31%, this means a zinc-rich ZnO material.

On the other hand, for Ta-doped ZnO samples; the formation of these structures could be explained as a similar form as undoped but instead of forming Zn liquid drops, it forms Zn–Ta alloy liquid drops. Because the difference of the fusion point between Zn (420 °C) and Ta (2996 °C) the properties of the alloy changes and it can affect the size and form of the deposited material, as seen in the sequence in Figure 6b–f. The higher the percentage of Ta_2O_5, the small structures are obtained. The shell is composed of small polyhedral crystals of ZnO material according to SEM, X-ray, and Raman measurements.

The crystals forming the shell were also affected by the introduction of Ta, as can be observed from FESEM in Figure 11b. The ZnO composing the shell had sheet-like polycrystalline shapes with a smaller crystallite size than the undoped ZnO (see Table 1).

The effect of both the decreased grain size and the change in the shape of the crystals in the ZnO:Ta-doped films was also observed and reported by different authors [40,41,56–58], and it was in

agreement with our experiments. This effect could be owing to the fact that tantalum atoms create a compression stress inside the lattice of ZnO, and they prevents an increase in these big shapes, as generated by the difference of ionic radii between Zn and Ta, as commented before in the XRD results. In fact, this phenomenon also has been observed when ZnO is doped with tantalum by other techniques [56], or when ZnO is doped with other materials such as aluminum and lithium [35,42].

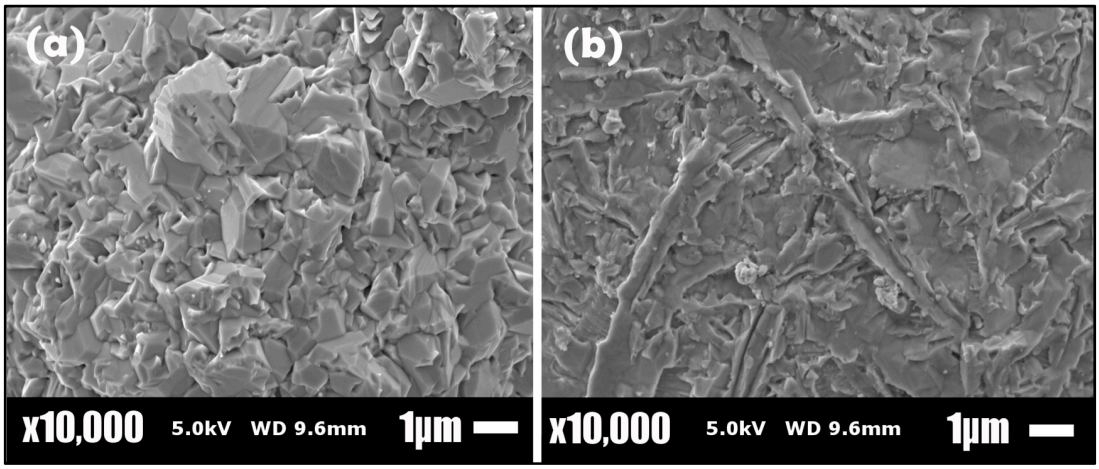

Figure 11. FESEM measurements on the shell from (**a**) undoped ZnO film, and (**b**) ZnO:Ta-doped film obtained with 300 mg of Ta_2O_5 in the pellet.

The synthesis of smaller structures means that somehow, the relation between the surface/volume of the film will increase, and this fact will be reflected in an increment of reactions between the existing species on the surface of structures, and also a possible increment in the adsorption and resorption of the species in these kind of porous films, and moreover, an increment of cations or anions on the surface of the film, as has been reported in other works; in fact, the role of the surface area has been observed to affect various mechanisms such as gas sensors, biological cells, and the effects of fluorescence emission [28,59–61].

3.4. Photoluminescence

The photoluminescence (PL) technique is a useful way to obtain information about the energy states of the impurities and defects of a material. Figure 12 shows the PL properties from our samples. As can be observed in that figure, all films exhibited two main bands, one sharp curve of around 380 nm, and another one with a more widened curve centered around 495 nm and extending from 425 nm to 625 nm. The PL intensity first increased as the percentage of Ta increased, and after that it decreased.

Photoluminescent emissions in ZnO were grouped into two main bands denominating the emissions near-band-edge (NBE), and deep-level emissions (DLE) corresponding to the transition band-to-band and the transition through to the deep centers, with energy levels in the forbidden gap, respectively. Emissions NBE in ZnO have been attributed to free excitation recombination, and they are observed at around the ultraviolet range.

Nevertheless, emissions DLE in ZnO have been assigned to the presence of various point defects, either intrinsic or extrinsic, which introduce deep levels in the bandgap and are assumed to be responsible for PL band broadening in the range between the blue and red emission [3,28,29,34,62].

As can be seen in Figure 12, the main PL band is the DLE band, and it increases in intensity by up to 60% as the Ta_2O_5 is incorporated into the growth process, and after that it reduces. Moreover, all bands are peaked at the same wavelength, independently of the percentage of Ta_2O_5, which means the doping with Ta does not seem to play a role in the generation of radiative deep centers other than for those of pure ZnO.

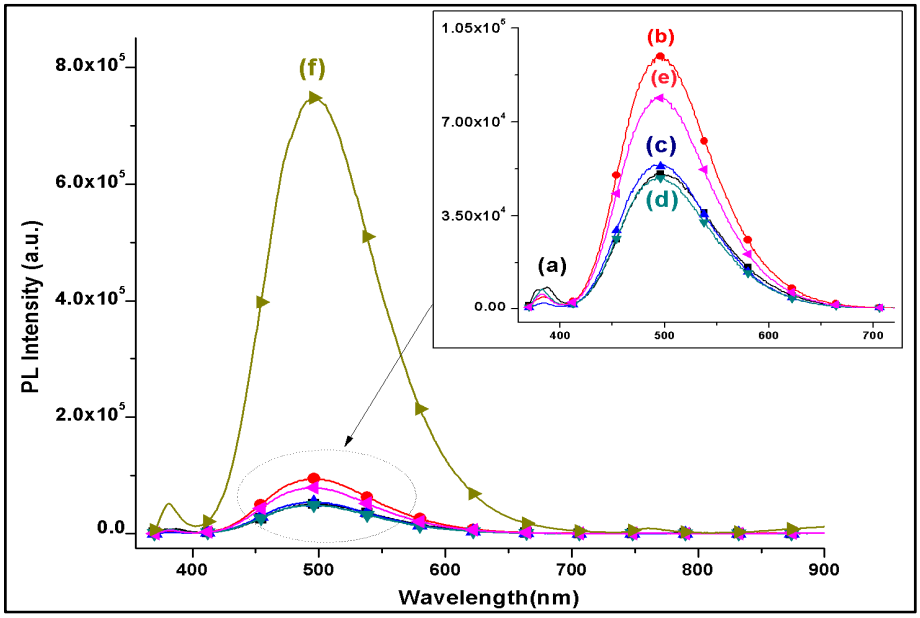

Figure 12. Photoluminescence spectra of (**a**) ZnO film and ZnO:Ta-doped films with (**b**) 10% Ta_2O_5, (**c**) 20% Ta_2O_5, (**d**) 40% Ta_2O_5, (**e**) 50% Ta_2O_5, and (**f**) 60% Ta_2O_5 in the pellet source.

To investigate the possible origin of the green luminescence observed in this type of films, many reports that try to describe this phenomena exactly, were reviewed, but there is no consensus, as the green emission has been observed on several films doped with Cu or Co atoms, on films with zinc vacancies (V_{Zn}), oxygen vacancies (V_O), interstitial zinc ions (Zn_i), oxygen antisites (O_{Zn}), and transitions $Zn_i \rightarrow V_{Zn}$, for these reasons, researchers came to the conclusion that this emission is a combination of several deep levels [62]. For example, in reference [63], it was reported that when ZnO films were annealed at temperatures higher than 800 °C, oxygen vacancies and zinc vacancies are generated, producing green emissions at 490 and 530 nm. In addition, a good correlation between the green emission and singly ionized oxygen vacancies was observed in commercial ZnO powders, annealed in forming gas (N_2:H_2) or O_2 at temperatures ranging from 500 to 1050 °C [64].

By other side, has been reported that either zinc vacancy and oxygen vacancy could contribute to green emission through shallow donors, and even Rodnyi and Khodyuk [62] reported that it is possible to assume the existence of donors with two levels (ground level and excited one) instead of two kinds of shallow donors. It has also been observed that in films of ZnO with an excess of oxygen, the maximum of the green luminescence is around 2.35 eV, and that zinc vacancies are responsible for the emission, but in ZnO films with an excess of zinc, the maximum of luminescence is around 2.53 eV, and in this case, oxygen vacancies acting as deep acceptor centers are responsible for the observed emission.

In our case, the DLE emission observed was centered at 2.53 eV, and according to the results presented above, the films contained both zinc in excess and oxygen vacancies; therefore, those defects could be involved in the PL phenomena.

As can be observed in Figure 12, all DLE emissions obtained in these films were centered at 2.50 eV (495 nm), and except for curve f, all films presented a broadening from 414 nm to 630 nm, and as mentioned above, the most intense peak could be attributed mainly to oxygen vacancies, and the broadening of curve could be assigned to a combination of different deep levels, either intrinsic or extrinsic.

Tantalum atoms introduced shallow donors in ZnO and modified its electrical conductivity, but in this case, those centers did not seem to play any effect on the PL phenomena, because zinc interstitials and oxygen vacancies are the defects involved in the PL phenomena.

Because the effect of the introduction of Ta atoms in ZnO is to increase the ratio of the volume to surface area as the structures area become smaller, the increase on the PL intensity could be attributed to a variation in the surface area of these films, as has been shown in the SEM section.

3.5. Hall Measurements

It is well-established that ZnO has natural type-n conductivity because of the formation of intrinsic defects, such as oxygen vacancies and zinc interstitials, during the synthesis. Oxygen vacancies can be easily formed and can contribute with two free electrons to the conduction band. However, it has been shown that those defects are actually deep donors, and they cannot contribute to the n-type conductivity. Therefore, zinc interstitials seem like the most probable defect acting as a donor in undoped ZnO films.

Carrier concentration, mobility, and the resistivity of films measured by the Hall–Vander Paw technique, are presented in Figure 13. The majority carrier mobility first increases up to a maximum value, and afterwards it reduces, as the Ta_2O_5 percentage is increased in the growth, while the carrier concentration increases as the Ta_2O_5 percentage increases.

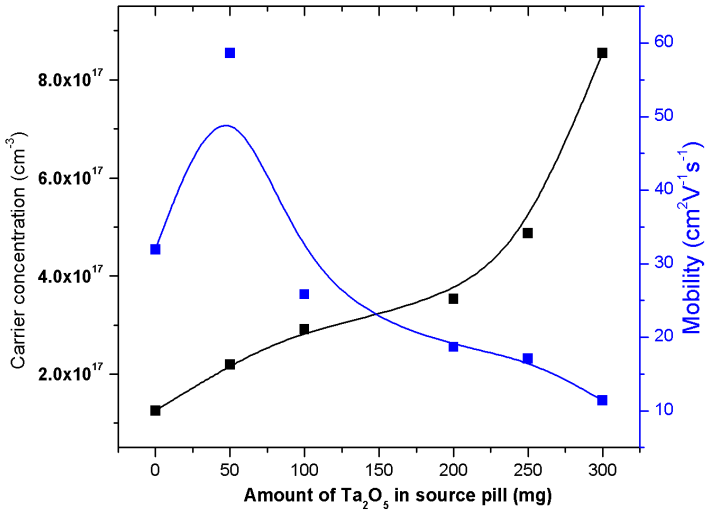

(**a**)

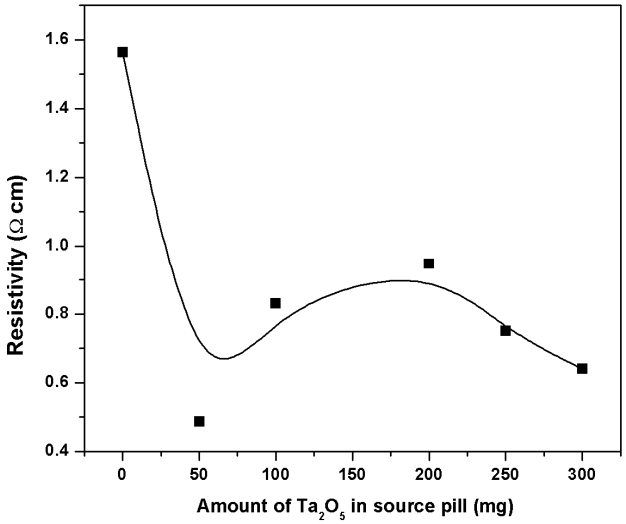

(**b**)

Figure 13. Electrical characterization of ZnO- and ZnO:Ta-doped films: (**a**) carrier concentration and mobility, and (**b**) resistivity.

The minimum value of the carrier concentration is for undoped samples (Figure 13a); therefore, the increase of the concentration was for the incorporation of the Ta atoms in the Zn positions of ZnO, and they contributed with electrons to the conduction band. The carrier concentration increased as the amount of Ta_2O_5 was incremented in the source pellet; this could be a clear reason for the increment in carrier concentration in ZnO:Ta-doped films, since if a tantalum atom replaces a zinc atom, this tantalum could have an oxidation state of $Ta1^+$, $Ta2^+$, or $Ta3^+$ with regards to Zn; this means that tantalum is capable of contributing with free electrons.

The mobility (Figure 13a) initially increased, with Ta_2O_5 reaching a maximum value in the film fabricated with 50 mg of Ta_2O_5 in the source; after that, it started to decrease. This effect has also been observed by Subha et al. [57,58], and is attributed to an excess of carriers in the ZnO lattice. A small increment observed in mobility, was owing to a high number of free carriers that were generated by tantalum atoms, and the relatively greater crystal size of the shell. Nevertheless, this mobility was reduced as the carrier concentration increased, because this carrier created a high number of collisions between them, besides the increase in the number of grain boundaries, due to a reduction in the crystal size in the shell. There are reports of ZnO with other dopants, in which it has been observed that foreign atoms inside the lattice of ZnO could act as charge trapping sites [33,42], which prevents the mobility of these free chargers. In our case, Ta atoms could be creating a similar effect, and therefore, the mobility in our films decreases with the amount of Ta_2O_5 in the source pellet.

With regard to the resistivity of the films, it can be appreciated in Figure 13b that initially for ZnO film, this had the highest value, but when these were doped with tantalum atoms, resistivity was around 0.5–1.0 Ωcm, but this tended to decrease, and this effect was attributed to an excess of carriers generated by donors from Ta atoms incorporated in the ZnO lattice.

For the conduction process in these type of films and to attempt to explain the results above the following, a model is proposed in Figure 14.

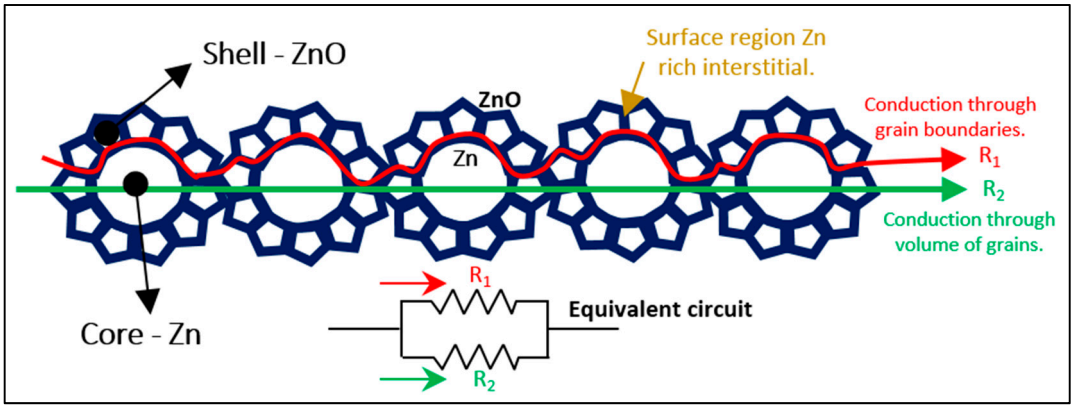

Figure 14. A model of conductivity through the crystal in the film. Two possible paths for conduction: intergrain (R_1) and through the volume of the grains (R_2).

First of all, we consider that the conduction of carriers in core shell structures could be a bit different from the pure crystals. As seen in the SEM pictures (Figure 9), the core shell structures were composed by a metallic core, and a shell formed by the oxide crystals. Due to the high temperature of the processes (above of the melting point of the zinc ~420 °C), the zinc atoms diffused through the grain boundaries to release the internal pressure, creating zinc-rich regions between grains. These zinc atoms became suboxides with a higher concentration of zinc interstitials at the surface than in the grain volume. The effect created a surface path for electric conduction, while the grain volume with lower concentrations of interstitials had a low contribution to the conductivity.

When tantalum was introduced into the ZnO matrix, the concentration of the carriers in the volume increased, and the grain was capable of being a transport carrier, and the resistivity of the film decreased, as shown in Figure 13.

4. Conclusions

ZnO- and ZnO:Ta-doped films were obtained through a HFCVD approach; the films were been obtained at 800 °C under a hydrogen atmosphere; the pellet source was fabricated with a powder mixture of ZnO and Ta_2O_5. The films obtained were studied for their structural, morphological, compositional, optical, and electrical properties; Ta atoms were incorporated into the ZnO wurtzite structure but they did not affect this crystal lattice, owing to the substitution of the Zn atoms with the Ta atoms, and these possess similar atomic radii; nevertheless, the Ta atoms tended to the growth direction (201) of ZnO. Raman spectroscopy confirms a majority contribution of ZnO in lattice, but Ta was not observed by this technique. According to EDS, from the films obtained, both ZnO- and ZnO:Ta-doped films are Zn-rich, but tantalum is present at a low concentration, though tantalum plays an important role in the morphological structure, and the roughness decreases as the amount of Ta is increased in the pellet source, and on the other hand, the density of the big sphere shapes tended to disappear; moreover, this technique confirms structures of a core–shell type. Photoluminescence studies reveal that the films obtained emit in a range of the green visible spectra, this effect mainly being due to oxygen vacancies; the tantalum atoms did not seem to play an important role in the creation of new centers of generation/recombination, but only in the intensity of emission observed in 495 nm; this was owing to the increment in the surface area of the films. Electrical measurements show that the films obtained are n-type, and that the tantalum atoms incorporated into the lattice of ZnO are contributing with a donor, increasing the carrier concentration as Ta is increased in the film; the resistivity and the sheet resistance also decrease when there is a greater amount of tantalum in the film.

Author Contributions: V.H. and T.D.-B. wrote, conceived and designed the experiments, E.R.-C., G.G.-S., and R.G. provide resources and systems to work, C.M., A.C., E.R., R.R., and F.G.N.-C. provide support in review and editing this work.

Acknowledgments: Authors gratefully acknowledge N. Rutilo Silva from IFUAP for FESEM images supported in this work, and M. Aceves from INAOE for PL measurements, as well as BUAP financial for support in publication fee, and CONACyT for Ph.D. support 304754 in the Institute of semiconductor devices program from BUAP.

Conflicts of Interest: The authors declare no conflict of interest. The funders had no role in the design of the study; in the collection, analyses, or interpretation of data; in the writing of the manuscript, and in the decision to publish the results.

References

1. Versteegh, M.A.M.; Vanmaekelbergh, D.; Dijkhuis, J.I. Room-Temperature Laser Emission of ZnO Nanowires Explained by Many-Body Theory. *Phys. Rev. Lett.* **2012**, *108*, 157402. [CrossRef] [PubMed]
2. Willander, M.; Nur, O.; Zhao, Q.X.; Yang, L.L.; Lorenz, M.; Cao, B.Q.; Ziga Pérez, J.; Czekalla, C.; Zimmermann, G.; Grundmann, M.; et al. Zinc oxide nanorod based photonic devices: Recent progress in growth, lightemitting diodes and lasers. *Nanotechnology* **2009**, *20*, 332001. [CrossRef] [PubMed]
3. Willander, M.; Nur, O.; Sadaf, J.R.; Qadir, M.I.; Zaman, S.; Zainelabdin, A.; Bano, N.; Hussain, I. Luminescence from zinc oxide nanostructures and polymers and their hybrid devices. *Materials* **2010**, *3*, 2643–2667. [CrossRef]
4. Guo, L.; Zhang, H.; Zhao, D.; Li, B.; Zhang, Z.; Jiang, M.; Shen, D. High responsivity ZnO nanowires based UV detector fabricated by the dielectrophoresis method. *Sens. Actuators B Chem.* **2012**, *166–167*, 12–16. [CrossRef]
5. Könenkamp, R.; Nadarajah, A.; Word, R.C.; Meiss, J.; Engelhardt, R. ZnO nanowires for LED and field-emission displays. *J. Soc. Inf. Disp.* **2008**, *16*, 609–613. [CrossRef]
6. Zheng, K.; Shen, H.; Li, J.; Sun, D.; Chen, G.; Hou, K.; Li, C.; Lei, W. The fabrication and properties of field emission display based on ZnO tetrapod-liked nanostructure. *Vacuum* **2008**, *83*, 261–264. [CrossRef]
7. Seelig, E.W.; Tang, B.; Yamilov, A.; Cao, H.; Chang, R.P.H. Self-assembeled 3D photonic crystals from ZnO colloidal spheres. *Mater. Chem. Phys.* **2002**, *9712*, 1–7.

8. Pietruszka, R.; Witkowski, B.S.; Gieraltowska, S.; Caban, P.; Wachnicki, L.; Zielony, E.; Gwozdz, K.; Bieganski, P.; Placzek-Popko, E.; Godlewski, M. New efficient solar cell structures based on zinc oxide nanorods. *Sol. Energy Mater. Sol. Cells* **2015**, *143*, 99–104. [CrossRef]
9. Vittal, R.; Ho, K.C. Zinc oxide based dye-sensitized solar cells: A review. *Renew. Sustain. Energy Rev.* **2017**, *70*, 920–935. [CrossRef]
10. Manthina, V.; Agrios, A.G. Band edge engineering of composite photoanodes for dye-sensitized solar cells. *Electrochim. Acta* **2015**, *169*, 416–423. [CrossRef]
11. Yazdi, M.A.P.; Martin, N.; Monsifrot, E.; Briois, P.; Billard, A. ZnO nano-tree active layer as heavy hydrocarbon sensor: From material synthesis to electrical and gas sensing properties. *Thin Solid Films* **2015**, *596*, 128–134. [CrossRef]
12. Chaudhary, S.; Umar, A.; Bhasin, K.K.; Baskoutas, S. Chemical sensing applications of ZnO nanomaterials. *Materials* **2018**, *11*, 287. [CrossRef] [PubMed]
13. Manthina, V.; Agrios, A.G. Single-pot ZnO nanostructure synthesis by chemical bath deposition and their applications. *Nano-Struct. Nano-Objects* **2016**, *7*, 1–11. [CrossRef]
14. Yang, P.F.; Wen, H.C.; Jian, S.R.; Lai, Y.S.; Wu, S.; Chen, R.S. Characteristics of ZnO thin films prepared by radio frequency magnetron sputtering. *Microelectron. Reliab.* **2008**, *48*, 389–394. [CrossRef]
15. Villanueva, Y.Y.; Liu, D.R.; Cheng, P.T. Pulsed laser deposition of zinc oxide. *Thin Solid Films* **2006**, *501*, 366–369. [CrossRef]
16. Lehraki, N.; Aida, M.S.; Abed, S.; Attaf, N.; Attaf, A.; Poulain, M. ZnO thin films deposition by spray pyrolysis: Influence of precursor solution properties. *Curr. Appl. Phys.* **2012**, *12*, 1283–1287. [CrossRef]
17. Wallace, R.; Brown, A.P.; Brydson, R.; Wegner, K.; Milne, S.J. Synthesis of ZnO nanoparticles by flame spray pyrolysis and characterisation protocol. *J. Mater. Sci.* **2013**, *48*, 6393–6403. [CrossRef]
18. Ohmagari, S.; Matsumoto, T.; Umezawa, H.; Mokuno, Y. Ohmic contact formation to heavily boron-doped p+ diamond prepared by hot-filament chemical vapor deposition. *MRS Adv.* **2016**, *1*, 3489–3495. [CrossRef]
19. Deshpande, S.; Dupuie, J.; Gulari, E. Filament-activated chemical vapour deposition of nitride thin films. *Adv. Mater. Opt. Electron.* **1996**, *6*, 135–146. [CrossRef]
20. Deshpande, S.V.; Dupuie, J.L.; Gualari, E. Hot filament assisted deposition of silicon nitride thin films. *Appl. Phys. Lett.* **1992**, *61*, 1420–1422. [CrossRef]
21. Silva-Andrade, F.; Chávez, F.; Gómez, E. Epitaxial GaAs growth using atomic hydrogen as the reactant. *J. Appl. Phys.* **1994**, *76*, 1946–1947. [CrossRef]
22. López, J.A.L.; López, J.C.; Valerdi, D.E.V.; Salgado, G.G.; Díaz-Becerril, T.; Pedraza, A.P.; Gracia, F.J.F. Morphological, compositional, structural, and optical properties of Si-nc embedded in SiOx films. *Nanoscale Res. Lett.* **2012**, *7*, 604. [CrossRef] [PubMed]
23. Mao, H.Y.; Lo, S.Y.; Wuu, D.S.; Wu, B.R.; Ou, S.L.; Hsieh, H.Y.; Horng, R.H. Hot-wire chemical vapor deposition and characterization of p-type nanocrystalline Si films for thin film photovoltaic applications. *Thin Solid Films* **2012**, *520*, 5200–5205. [CrossRef]
24. Mendoza, F.; Limbu, T.B.; Weiner, B.R.; Morell, G. Large-area bilayer graphene synthesis in the hot filament chemical vapor deposition reactor. *Diam. Relat. Mater.* **2015**, *51*, 34–38. [CrossRef]
25. Wang, B.B.; Zhu, M.K.; Ostrikov, K.; Shao, R.W.; Zheng, K. Structure and photoluminescence of molybdenum selenide nanomaterials grown by hot filament chemical vapor deposition. *J. Alloys Compd.* **2015**, *647*, 734–739. [CrossRef]
26. Mortazavi, S.H.; Ghoranneviss, M.; Dadashbaba, M.; Alipour, R. Synthesis and investigation of silicon carbide nanowires by HFCVD method. *Bull. Mater. Sci.* **2016**, *39*, 953–960. [CrossRef]
27. Ramos, J.R.; Morales, C.; García, G.; Díaz, T.; Rosendo, E.; Santoyo, J.; Oliva, A.I.; Galeazzi, R. Optical and structural analysis of ZnS core-shell type nanowires. *J. Alloys Compd.* **2018**, *736*, 93–98. [CrossRef]
28. Janotti, A.; Van De Walle, C.G. Native point defects in ZnO. *Phys. Rev. B Condens. Matter Mater. Phys.* **2007**, *76*, 165202. [CrossRef]
29. Jayakumar, O.D.; Sudarsan, V.; Sudakar, C.; Naik, R.; Vatsa, R.K.; Tyagi, A.K. Green emission from ZnO nanorods: Role of defects and morphology. *Scr. Mater.* **2010**, *62*, 662–665. [CrossRef]
30. Gahlaut, U.P.S.; Kumar, V.; Pandey, R.K.; Goswami, Y.C. Highly luminescent ultra small Cu doped ZnO nanostructures grown by ultrasonicated sol-gel route. *Optik* **2016**, *127*, 4292–4295. [CrossRef]

31. Wang, Y.; Liu, N.; Chen, Y.; Yang, C.; Liu, W.; Su, J.; Li, L.; Gao, Y. Multicolour electroluminescence from light emitting diode based on ZnO:Cu/p-GaN heterojunction at positive and reverse bias voltage. *RSC Adv.* **2015**, *5*, 104386–104391. [CrossRef]
32. Muthukumaran, S.; Gopalakrishnan, R. Structural, FTIR and photoluminescence studies of Cu doped ZnO nanopowders by co-precipitation method. *Opt. Mater.* **2012**, *34*, 1946–1953. [CrossRef]
33. Klingshirn, C. ZnO: From basics towards applications. *Phys. Status Solidi Basic Res.* **2007**, *244*, 3027–3073. [CrossRef]
34. Özgür, Ü.; Alivov, Y.I.; Liu, C.; Teke, A.; Reshchikov, M.A.; Doğan, S.; Avrutin, V.; Cho, S.J.; Morkoç, H. A comprehensive review of ZnO materials and devices. *J. Appl. Phys.* **2005**, *98*, 1–103. [CrossRef]
35. Chitra, M.; Uthayarani, K.; Rajasekaran, N.; Girija, E.K. Preparation and characterisation of Al doped ZnO nanopowders. *Phys. Procedia* **2013**, *49*, 177–182. [CrossRef]
36. Liu, M.; Kitai, A.H.; Mascher, P. Point defects and luminescence centers in zinc oxide and zinc oxide doped with manganese. *J. Lumin.* **1992**, *54*, 35–42. [CrossRef]
37. López, R.; Díaz, T.; García, G.; Rosendo, E.; Galeazzi, R.; Coyopol, A.; Juárez, H.; Pacio, M.; Morales, F.; Oliva, A.I. Fast formation of surface Oxidized Zn Nanorods and urchin-like microclusters. *Adv. Mater. Sci. Eng.* **2014**, *2014*. [CrossRef]
38. Richard, D.; Romero, M.; Faccio, R. Experimental and theoretical study on the structural, electrical and optical properties of tantalum-doped ZnO nanoparticles prepared via sol-gel acetate route. *Ceram. Int.* **2018**, *44*, 703–711. [CrossRef]
39. Yuan, L.; Wang, C.; Cai, R.; Wang, Y.; Zhou, G. Temperature-dependent growth mechanism and microstructure of ZnO nanostructures grown from the thermal oxidation of zinc. *J. Cryst. Growth* **2014**, *390*, 101–108. [CrossRef]
40. Cheng, Y.; Cao, L.; He, G.; Yao, G.; Song, X.; Sun, Z. Preparation, microstructure and photoelectrical properties of Tantalum-doped zinc oxide transparent conducting films. *J. Alloys Compd.* **2014**, *608*, 85–89. [CrossRef]
41. Krishnan, R.R.; Vinodkumar, R.; Rajan, G.; Gopchandran, K.G.; Mahadevan Pillai, V.P. Structural, optical, and morphological properties of laser ablated ZnO doped Ta_2O_5 films. *Mater. Sci. Eng. B Solid-State Mater. Adv. Technol.* **2010**, *174*, 150–158. [CrossRef]
42. Bang, K.; Son, G.C.; Son, M.; Jun, J.H.; An, H.; Baik, K.H.; Myoung, J.M.; Ham, M.H. Effects of Li doping on the structural and electrical properties of solution-processed ZnO films for high-performance thin-film transistors. *J. Alloys Compd.* **2018**, *739*, 41–46. [CrossRef]
43. Khan, A. Raman Spectroscopic Study of the ZnO Nanostructures. *J. Pak. Mater. Soc.* **2010**, *4*, 5–9.
44. Schumm, M. ZnO-Based Semiconductors Studied by Raman Spectroscopy: Semimagnetic Alloying, Doping, and Nanostructures. Ph.D. Thesis, Julius–Maximilians University, Würzburg, Germany, July 2008.
45. Soosen, S.M.; Koshy, J.; Chandran, A.; George, K.C. Optical phonon confinement in ZnO nanorods and nanotubes. *Indian J. Pure Appl. Phys.* **2010**, *48*, 703–708.
46. Zhang, R.; Yin, P.G.; Wang, N.; Guo, L. Photoluminescence and Raman scattering of ZnO nanorods. *Solid State Sci.* **2009**, *11*, 865–869. [CrossRef]
47. Tzolov, M.; Tzenov, N.; Dimova-Malinovska, D.; Kalitzova, M.; Pizzuto, C.; Vitali, G.; Zollo, G.; Ivanov, I. Vibrational properties and structure of undoped and Al-doped ZnO films deposited by RF magnetron sputtering. *Thin Solid Films* **2000**, *379*, 28–36. [CrossRef]
48. Goff, A.H.-L.; Joiret, S.; Saïdani, B.; Wiart, R. In-situ Raman spectroscopy applied to the study of the deposition and passivation of zinc in alkaline electrolytes. *J. Electroanal. Chem.* **1989**, *263*, 127–135. [CrossRef]
49. Marchebois, H.; Joiret, S.; Savall, C.; Bernard, J.; Touzain, S. Characterization of zinc-rich powder coatings by EIS and Raman spectroscopy. *Surf. Coat. Technol.* **2002**, *157*, 151–161. [CrossRef]
50. Janotti, A.; Van De Walle, C.G. Fundamentals of zinc oxide as a semiconductor. *Rep. Prog. Phys.* **2009**, *72*, 126501. [CrossRef]
51. Van De Walle, C.G.; Neugebauer, J. First-principles calculations for defects and impurities: Applications to III-nitrides. *J. Appl. Phys.* **2004**, *95*, 3851–3879. [CrossRef]
52. López, R.; García, G.; Díaz, T.; Coyopol, A.; Rosendo, E.; Galeazzi, R.; Juárez, H.; Pacio, M. Low temperature growth of Zn-ZnO microspheres by atomic hydrogen assisted-HFCVD. *IOP Conf. Ser. Mater. Sci. Eng.* **2013**, *45*, 012016. [CrossRef]

53. López, R.; Díaz, T.; García, G.; Galeazzi, R.; Rosendo, E.; Coyopol, A.; Pacio, M.; Juárez, H.; Oliva, A.I. Structural properties of Zn-ZnO core-shell microspheres grown by hot-filament CVD technique. *J. Nanomater.* **2012**, *2012*, 865321. [CrossRef]
54. Lin, J.H.; Patil, R.A.; Devan, R.S.; Liu, Z.A.; Wang, Y.P.; Ho, C.H.; Liou, Y.; Ma, Y.R. Photoluminescence mechanisms of metallic Zn nanospheres, semiconducting ZnO nanoballoons, and metal-semiconductor Zn/ZnO nanospheres. *Sci. Rep.* **2014**, *4*, 6967. [CrossRef] [PubMed]
55. Zhao, C.X.; Li, Y.F.; Zhou, J.; Li, L.Y.; Deng, S.Z.; Xu, N.S.; Chen, J. Large-scale synthesis of bicrystalline ZnO nanowire arrays by thermal oxidation of zinc film: Growth mechanism and high-performance field emission. *Cryst. Growth Des.* **2013**, *13*, 2897–2905. [CrossRef]
56. Wu, Y.; Li, C.; Li, M.; Li, H.; Xu, S.; Wu, X.; Yang, B. Microstructural and optical properties of Ta-doped ZnO films prepared by radio frequency magnetron sputtering. *Ceram. Int.* **2016**, *42*, 10847–10853. [CrossRef]
57. Ravichandran, K.; Subha, K.; Dineshbabu, N.; Manivasaham, A. Enhancing the electrical parameters of ZnO films deposited using a low-cost chemical spray technique through Ta doping. *J. Alloys Compd.* **2016**, *656*, 332–338. [CrossRef]
58. Subha, K.; Ravichandran, K.; Sriram, S. Combined influence of fluorine doping and vacuum annealing on the electrical properties of ZnO:Ta films. *Appl. Surf. Sci.* **2017**, *409*, 413–425. [CrossRef]
59. Li, G.; Kawi, S. High-surface-area SnO: A novel semiconductor-oxide. *Mater. Lett.* **1998**, *34*, 99–102. [CrossRef]
60. Bain, L.E.; Collazo, R.; Hsu, S.H.; Latham, N.P.; Manfra, M.J.; Ivanisevic, A. Surface topography and chemistry shape cellular behavior on wide band-gap semiconductors. *Acta Biomater.* **2014**, *10*, 2455–2462. [CrossRef] [PubMed]
61. Soni, U.; Sapra, S. The Importance of Surface in Core—Shell Semiconductor Nanocrystals. *J. Phys. Chem.* **2010**, *114*, 22514–22518. [CrossRef]
62. Rodnyi, P.A.; Khodyuk, I.V. Optical and luminescence properties of zinc oxide (Review). *Opt. Spectrosc.* **2011**, *111*, 776–785. [CrossRef]
63. Studenikin, S.A.; Golego, N.; Cocivera, M. Fabrication of green and orange photoluminescent, undoped ZnO films using spray pyrolysis. *J. Appl. Phys.* **1998**, *84*, 2287–2294. [CrossRef]
64. Vanheusden, K.; Warren, W.L.; Seager, C.H.; Tallant, D.R.; Voigt, J.A.; Gnade, B.E. Mechanisms behind green photoluminescence in ZnO phosphor powders. *J. Appl. Phys.* **1996**, *79*, 7983–7990. [CrossRef]